14th International Symposium on Turbulence and Shear Flow Phenomena (TSFP14)
Heidelberg, Germany, July 28–31, 2026

STABILITY ANALYSIS OF BLASIUS BOUNDARY LAYER VIA STRUCTURED SMALL-GAIN THEOREM

Ofek Frank-Shapir
The Stephen B. Klein Faculty of Aerospace Engineering
Technion – Israel Institute of Technology
Haifa, 3200003, Israel
ofekfr@campus.technion.ac.il

Igal Gluzman
The Stephen B. Klein Faculty of Aerospace Engineering
Technion – Israel Institute of Technology
Haifa, 3200003, Israel
igal.gluzman@technion.ac.il

ABSTRACT

This work presents a structured input-output framework for stability analysis of finite-magnitude disturbances. The Navier-Stokes equations are represented as an interconnected linearized system with structured feedback uncertainty to model the advection term via structured singular values. Herein, we propose a representation of such an interconnected system that allows for preserving the structure of the advection term while maintaining efficient computation. Then, by applying a structured small-gain theorem to our representation of the interconnected system, we provide an explicit threshold on the magnitude of velocity perturbations that assures flow stability. We demonstrate the application of our stability analysis approach on the Blasius boundary layer under finite-size perturbations. The results show that these thresholds decrease as the Reynolds number increases, where streak-related modes govern the threshold at lower Reynolds numbers, while the Tollmien–Schlichting mode becomes dominant near the critical Reynolds number.

INTRODUCTION

Understanding the stability of shear flows in the presence of finite-magnitude disturbances remains a central challenge in transition research. Classical linear stability theory (LST) predicts the onset of instability under infinitesimal perturbations, and has been highly successful in identifying modal instability mechanisms via eigenvalue analysis, such as Tollmien–Schlichting (TS) waves. However, many transitional flows are known to exhibit strong sensitivity to finite-amplitude disturbances, in which subcritical transition may arise through mechanisms not captured by purely linear modal analysis. In boundary layers, for example, oblique-wave interactions and streak-related structures play a major role in bypass transition and may dominate the route to instability well below the critical Reynolds number predicted by LST.

Input-output analysis has emerged as a useful framework for studying disturbance amplification in shear flows, characterizing how forcing is amplified by the linearized Navier-Stokes dynamics. Examples include studies that focused on the externally forced LNS equations to examine dynamic processes, structural features, and energy pathways for a variety of base flows (Farrell & Ioannou, 1993; Bamieh & Dahleh, 2001; Jovanović & Bamieh, 2004, 2005; Hwang & Cossu, 2010; McKeon & Sharma, 2010; McKeon *et al.*, 2013; McKeon, 2017; Madhusudanan *et al.*, 2019; Liu & Gayme, 2020; Symon *et al.*, 2021) and including recent studies, where the dynamics of large-scale structures in turbulent boundary layer are studied by analyzing the flow response to external periodic perturbations (Liu *et al.*, 2022), and utilization of input-output approach for modeling different actuation geometry patterns (Gluzman & Gayme, 2021; Frank-Shapir & Gluzman, 2025). More recently, structured input-output methodologies have extended this framework by modeling the nonlinear term as structured feedback uncertainty and quantifying worst-case amplification via structured singular values (SSVs) (Liu & Gayme, 2021; Mushtaq *et al.*, 2023; Shuai *et al.*, 2023; Mushtaq *et al.*, 2024). This approach, coupled with the small-gain theorem, enables the derivation of stability criteria, which allow accounting for the presence of finite-amplitude disturbances in the shear flow, as shown in our recent work (Frank-Shapir & Gluzman, 2026).

A key difficulty within structured input-output analysis is faithfully representing the advection term by the uncertainty structure. In structured input–output analysis, the nonlinear term in the NSE is modeled as a fixed-structure uncertainty that is interconnected with the linear frequency-response operator obtained from the LNS equations. Previous structured input-output studies have employed two uncertainty modeling approaches: non-repeated blocks (Liu & Gayme, 2021) and repeated blocks (Mushtaq *et al.*, 2023), used to obtain tractable SSV computations (Liu & Gayme, 2021; Mushtaq *et al.*, 2023; Shuai *et al.*, 2023; Mushtaq *et al.*, 2024; Frank-Shapir & Gluzman, 2026). While such approximations have been proven to provide valuable insights, they do not preserve the exact structure of the nonlinear advection term in the Navier-Stokes equations and thus may include additional feedback pathways that are not physically associated with the effect of the advection term on the flow, leading to a stricter bound on the disturbance threshold to maintain the stability of the interconnected system. The primary obstacle to preserving the exact structure of the advection term is the complex set of constraints involved, which makes the process computationally prohibitive.

Herein, we propose a new structured input-output formulation of the NSE to represent the structure of the advection while remaining computationally feasible. We utilize our new structure within a structured small-gain theorem approach, which yields explicit bounds on admissible perturbation velocity, allowing stability analysis to be assessed directly in terms of disturbance magnitude. Using this approach, we examine how disturbance thresholds vary with Reynolds number and wavenumber pair in the incompressible Blasius boundary layer, showing that our new structure yields less restrictive bounds than previous structured input-output approaches.

MATHEMATICAL MODEL

We consider incompressible shear flow, for which the linearized Navier-Stokes equations for perturbations in fluid velocity and pressure (u,p) about the base flow $(\overline{u},\overline{p})$ are as follows:

$$\begin{aligned} \frac{\partial u}{\partial t} &= -\bar{u}\cdot\nabla u - u\cdot\nabla\bar{u} - \nabla p + \frac{1}{Re}\Delta u + d, \\ \nabla\cdot u &= 0. \end{aligned} \tag{1}$$

Here, $u = \begin{bmatrix} u \ v \ w \end{bmatrix}^T$ is the velocity perturbation vector, corresponding to the streamwise x, wall-normal y, and spanwise z directions, respectively. Throughout this letter, we consider Blasius flow (illustrated in Fig. 1) with a base velocity profile of the form $\overline{u} = \begin{bmatrix} U(y) \ 0 \ 0 \end{bmatrix}^T$, where $U(y)$ is obtained numerically by solving the Blasius equation $f''' + ff'' = 0$ (Schlichting & Gersten, 2016), where f' is the normalized base flow velocity varying as a function of the similarity variable $\eta = y/\delta^*$, where δ^* is the displacement thickness. The boundary conditions used for the solution of the Blasius equation are $f(0) = f'(0) = 0$ and $\lim_{\eta\to\infty} f'(\eta) = 1$. The Reynolds number is $Re = \mathscr{U}\delta^*/\nu$, where $\mathscr{U}$ is freestream velocity, δ^* is the displacement thickness, and ν is the kinematic viscosity of the fluid. These parameters are also used to render the variables dimensionless. Additionally, $d = \begin{bmatrix} d_x \ d_y \ d_z \end{bmatrix}^T$ is the term representing body forcing, ∇ is the del operator and $\Delta \equiv \nabla^2$ is the Laplacian operator.

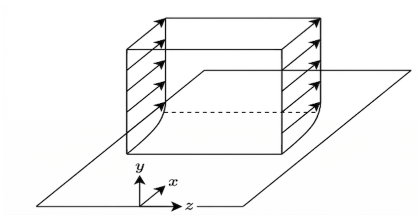

Figure 1: Illustration of Blasius boundary layer flow.

Next, the LNS equations are written in a state-space form, which simplifies performing input-output analysis via a formulation similar to the one in Jovanović & Bamieh (2005):

$$\begin{aligned} \frac{\partial\psi}{\partial t}(k_x,y,k_z,t) &= [\mathscr{A}(k_x,k_z)\psi(k_x,k_z,t)](y) \\ &\quad + [\mathscr{B}(k_x,k_z)d(k_x,k_z,t)](y), \\ \phi(k_x,y,k_z,t) &= [\mathscr{C}(k_x,k_z)\psi(k_x,k_z,t)](y), \end{aligned} \tag{2}$$

where $\psi \equiv \begin{bmatrix} v \ \omega_y \end{bmatrix}^T$. Here, v is the velocity perturbation in wall-normal direction, $\omega_y = \partial u/\partial z - \partial w/\partial x$ is the wall-normal vorticity component, and the forcing term is denoted as d. $\phi \equiv \mathbf{u}$ is the system output, which is set to be the velocity perturbation vector. Spatial invariance is assumed in the horizontal directions under a quasi-parallel assumption for Blasius flow, which allows us to apply the Fourier transform in the x and z directions, yielding a system of 2 PDEs in Eq. (2) in terms of the spatial wavenumbers k_x, k_z, and y, the wall-normal position. The input to output frequency response operator representation of the above system is

$$\begin{aligned} &\mathscr{H}_\nabla(y;k_x,k_z,\omega) = \\ &\mathrm{diag}(\nabla,\nabla,\nabla)[\mathscr{C}(k_x,k_z)[i\omega I - \mathscr{A}(k_x,k_z)]^{-1}\mathscr{B}(k_x,k_z)](y), \end{aligned} \tag{3}$$

where the details on the explicit form of the operators denoted as $\mathscr{A}$, $\mathscr{B}$, and $\mathscr{C}$, and ∇ can be found in Jovanović & Bamieh (2005).

We model the nonlinear advection term introduced to the linearized system as an external forcing with the following form: $f = -\mathbf{u}_\Xi \cdot \mathrm{diag}(\nabla,\nabla,\nabla)\mathbf{u}$, where $\mathbf{u}_\Xi$ is a fixed matrix feedback gain that has a certain structure in the interconnected system shown in Fig. 2a. Structure constraints are imposed to limit feedback pathways for the goal of replicating the structure of the nonlinearity in the NSE, which is treated in the SSV framework as modeling uncertainty. The structure constraints

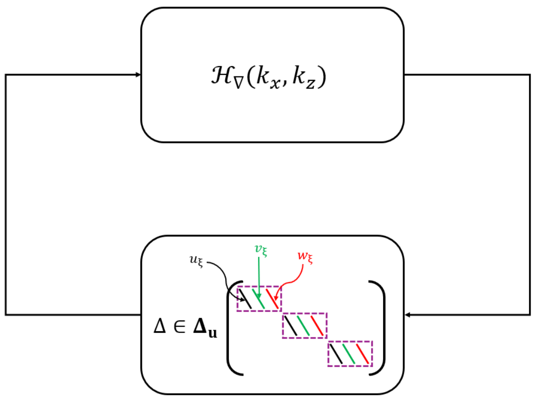

(a)

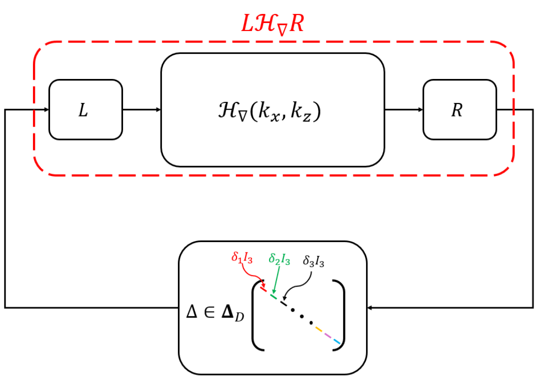

(b)

Figure 2: Representations of the NSE via: (a) Interconnection loop block diagram with uncertainty structure $\Delta_{\mathbf{u}}$. (b) Our modified block diagram with uncertainty structure $\Delta_{\mathbf{D}}$.

are imposed by calculating SSVs for the frequency response operator $\mathscr{H}_\nabla$ by solving the following minimization problem (Packard & Doyle, 1993; Zhou *et al.*, 1995):

$$\mu_\Delta[\mathscr{H}_\nabla(k_x,k_z,\omega)] = \frac{1}{M_\Delta}, \tag{4a}$$

$$M_\Delta \equiv \min\{\overline{\sigma}(\mathbf{U}_\Xi) : \mathbf{U}_\Xi \in \Delta, \det[I - \mathscr{H}_\nabla \mathbf{U}_\Xi] = 0\}. \tag{4b}$$

Here, we consider a discretized version of $\mathbf{u}_\Xi$, which we denote as a constant-valued matrix $\mathbf{U}_\Xi$. Here, $\overline{\sigma}(\cdot)$ represents the largest singular value, $\det[\cdot]$ is the determinant of a matrix, and Δ is a set of matrices that includes all the matrices that have a certain structure. In this framework, the matrix $\mathbf{U}_\Xi$ is not known apriori. Rather, it is computed by solving Eq. (4) such that it is the smallest structured uncertainty (in terms of the largest singular value) that will cause instability of the system.

We quantify amplification with nonlinear interactions that are modeled by a structured uncertainty $\mathbf{U}_\Xi \in \Delta$ using the supremum over all temporal frequencies, i.e.

$$\|\mathscr{H}_\nabla\|_{\mu_\Delta}(k_x,k_z) = \sup_{\omega\in\mathbb{R}} \mu_\Delta[\mathscr{H}_\nabla(k_x,k_z,\omega)], \tag{5}$$

which is the "worst-case" amplification of perturbation gradients under the uncertainty structure Δ. Additionally, we use the notation $\|\cdot\|_{\mu_\Delta}$ for consistency with previous works (Packard & Doyle, 1993; Liu & Gayme, 2021; Frank-Shapir & Gluzman, 2026), even though this operator is not a proper norm because it does not satisfy the triangle inequality.

Using the small-gain theorem, the following condition for system stability is proposed in Frank-Shapir & Gluzman (2026),

$$\max_{y\in\mathscr{Y}} \|\mathbf{u}(y)\|_2 < \|\mathscr{H}_\nabla\|^{-1}_{\mu_{\Delta_\mathbf{u}}}(k_x,k_z). \tag{6}$$

Here, $\max_{y\in\mathscr{Y}} \|\mathbf{u}(y)\|_2$ represents the largest velocity perturbation found in the wall-normal domain $\mathscr{Y}$. Eq. (6) provides a bound of value $\|\mathscr{H}_\nabla\|^{-1}_{\mu_\Delta}$ on the magnitude of perturbations that are allowed in the flow to maintain stability.

UNCERTAINTY STRUCTURE

The uncertainty structure that approximates $\mathbf{u}_\Xi$, for reproducing the structure of the advection term in the NSE, within the interconnected system shown in Fig. 2a, is

$$\Delta_\mathbf{u} = \left\{ \begin{bmatrix} \Delta_u & \mathbf{0} & \mathbf{0} \\ \mathbf{0} & \Delta_u & \mathbf{0} \\ \mathbf{0} & \mathbf{0} & \Delta_u \end{bmatrix}, \Delta_u = [\mathrm{diag}(u_\xi), \mathrm{diag}(v_\xi), \mathrm{diag}(w_\xi)] \right\}. \tag{7}$$

Here, $u_\xi, v_\xi, w_\xi \in \mathbb{C}^{N_y\times 1}$ and N_y is the number of points that are used in the discretization of the wall-normal direction. Any additional terms that are not included in the set $\mathbf{\Delta_u}$ may be regarded as fictitious amplification pathways that are not associated with the structure of the non-linear advection term of the NSE (within a structured input-output framework) and, thus, do not represent physical flow behaviors.

The solution for uncertainties in $\mathbf{\Delta_u}$ involves the solution of the optimization problem in Eq. (4) with a very complex set of constraints that are required for preserving the structure in Eq. (7). Such a solution has not yet been found, as far as we know. Previous works in the field of structured input-output analysis employ different, only simplified approximations for the structure of $\mathbf{U}_\Xi$, namely uncertainty with non-repeated blocks (Liu & Gayme, 2021), and repeated blocks (Mushtaq *et al.*, 2024) without preserving the exact structure in Eq. (7).

In our study, we propose a novel representation of the interconnected system, which is used to model the NSE in Fig. 2a, via modifying the transfer function $\mathscr{H}_\nabla$ to efficiently compute SSVs while preserving the amplification pathways that are associated with the structure in Eq. (7). This process is described in Fig. 2b, where we apply the transformation represented by the matrices L and R to the frequency operator $\mathscr{H}_\nabla$, such that $\mathbf{U}_\Xi \in \Delta_\mathbf{u}$ and $\mathbf{U}_\Xi = L\mathbf{V}_\Xi R$, where $\mathbf{V}_\Xi$ is a new uncertainty matrix satisfying $\mathbf{V}_\Xi \in \Delta_D$ and the details on the two matrices L and R are provided in Appendix A. The result of this transformation is shown in Fig. 2b. This in turn allows us to consider the simplified uncertainty structure, denoted as Δ_D, which is defined as follows:

$$\Delta_D = \{\mathrm{diag}(\delta_1 I_3, \ldots, \delta_{3N_y} I_3) : \delta_i \in \mathbb{C}\}. \tag{8}$$

Here, $\delta_i \in \mathbb{C}$ are scalar quantities, where $i = 1,2,...,3N_y$, and I_3 is a 3×3 identity matrix. By using this transformation, we obtain the following relation between $\|\mathscr{H}_\nabla\|_{\mu_\Delta}$ and $\|R\mathscr{H}_\nabla L\|_{\mu_{\Delta_D}}$ (for details see Appendix A),

$$\|\mathscr{H}_\nabla\|^{-1}_{\mu_{\Delta_\mathbf{u}}} \leq \sqrt{3}\|R\mathscr{H}_\nabla L\|^{-1}_{\mu_{\Delta_D}}, \tag{9}$$

where $\|R\mathscr{H}_\nabla L\|_{\mu_{\Delta_D}}$ is computationally feasible to obtain. We use this result to determine the stability threshold on velocity perturbation magnitude, based on Eq. (6)

$$\max_{y\in\mathscr{Y}} \|\mathbf{u}(y)\|_2 < \sqrt{3}\|R\mathscr{H}_\nabla L\|^{-1}_{\mu_{\Delta_D}}, \tag{10}$$

The relation in Eq. (10) is suggested to be used for stability analysis within the structured small-gain theorem framework in Frank-Shapir & Gluzman (2026), providing a less conservative bound that is closer to the $\|\mathscr{H}_\nabla\|^{-1}_{\mu_{\Delta_\mathbf{u}}}$ bound compared to bounds that are determined via repeated and non-repeated block approaches.

RESULTS

In this section, we utilize the new suggested bound on the disturbance threshold for Blasius flow. In this process, SSVs are computed using the matrix set Δ_D, via the MATLAB function *mussv*. A discretization is applied in the wall-normal direction with $N = 31$ Chebyshev discretization points, whereas for the wavenumber domain, we used a 50×90 grid of logarithmically spaced values with the following boundaries: $(k_{x_{min}} = 10^{-4}, k_{x_{max}} = 3.02)$ and $(k_{z_{min}} = 10^{-2}, k_{z_{max}} = 15.84)$, which are the same as in Jovanović & Bamieh (2005) and were found to be sufficient to obtain reliable converged results.

We examine and analyze here the contour plots of $\sqrt{3}\|R\mathscr{H}_\nabla L\|^{-1}_{\mu_{\Delta_D}}$ over the k_x, k_z domain at specific Reynolds numbers. With this approach, we identify modes of interest that determine the stability threshold bound in our analysis. Next, we analyze the behavior of three pre-selected modes across a wide range of Reynolds numbers, which we identified as dominant modes based on the results of Fig. 3. We focus on three specific modes where each mode is represented by a unique wave number pair (k_x, k_z). Specifically, the considered modes are listed in Table 1.

OW	$(k_x, k_z) = (0.104, 0.12)$
TS	$(k_x, k_z) = (0.298, 10^{-2})$
SPS	$(k_x, k_z) = (10^{-4}, 0.13)$

Table 1: Selected modes: OW - oblique wave, TS - Tollmien–Schlichting, SPS - spanwise periodic streak.

In Fig. 3, we show the contour maps of $\sqrt{3}\|R\mathscr{H}_\nabla L\|^{-1}_{\mu_{\Delta_D}}(k_x, k_z)$, for the Reynolds numbers $Re = 300$ (Fig. 3a) and $Re = 500$ (Fig. 3b). Over these contour maps, we overlay the modes from Table 1. The most dominant mode (that is associated with the lowest stability threshold) is marked with an X symbol. In Fig. 3a, the smallest perturbation magnitude corresponding to one of the contours is $10^{-2.6} \approx 2.5 \times 10^{-3}$, while the smallest perturbation magnitude in Fig. 3b is $10^{-3.4} \approx 4 \times 10^{-4}$. This observation is consistent with the results shown in Frank-Shapir & Gluzman (2026), indicating that boundary-layer flow can become unstable under smaller perturbations as the Reynolds number increases. Additionally, the most dominant flow structure—the mode that is associated with the lowest bound on perturbation magnitude—changes with the Reynolds number. For Reynolds numbers significantly lower than $Re_c = 520$, the critical value predicted by LST (Schmid & Henningson, 2001), the dominant flow structure is an oblique wave as shown in Fig. 3a. In contrast, Fig. 3b shows that closer to $Re_c = 520$, the dominant flow structure changes, and becomes the TS mode. This result is consistent with observations in Frank-Shapir & Gluzman (2026) for other uncertainty structures.

Next, in Fig. 4, we show the evolution of the imposed bounds $\sqrt{3}\|R\mathscr{H}_\nabla L\|^{-1}_{\mu_{\Delta_D}}$ computed via our approach (denoted by solid curves) as a function of Reynolds number over the wide range, $Re \in [100, 520]$ for the pre-selected modes that are listed in Table 1. We also compute and show on the same plot the bounds that we denote as $\|\mathscr{H}_\nabla\|^{-1}_{\mu_{\Delta_r}}$ (via dashed curves) using the repeated blocks uncertainty structure that was suggested by Mushtaq *et al.* (2024). The following insights can be drawn from this plot.

First, for each respective mode we observe that $\|\mathscr{H}_\nabla\|^{-1}_{\mu_{\Delta_r}} < \sqrt{3}\|R\mathscr{H}_\nabla L\|^{-1}_{\mu_{\Delta_D}}$. This result is to be expected, as we suggest a bound aimed to be closer to the $\|\mathscr{H}_\nabla\|^{-1}_{\mu_{\Delta_\mathbf{u}}}$ bound compared to bounds obtained via the repeated-block approach. Therefore, a less conservative uncertainty structure leads to less conservative stability estimates, as explained in Frank-Shapir & Gluzman (2026).

Second, the curve corresponding to the TS mode rapidly decreases from $Re \approx 400$, approaching zero at $Re = 520$. At Reynolds numbers approaching $Re = 520$, the threshold $\sqrt{3}\|R\mathscr{H}_\nabla L\|^{-1}_{\mu_{\Delta_D}}$ approaches infinitesimal values, which corresponds to the flow being unstable even for asymptotically

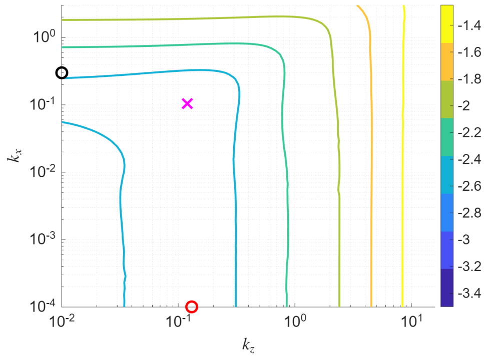

(a) $Re = 300$

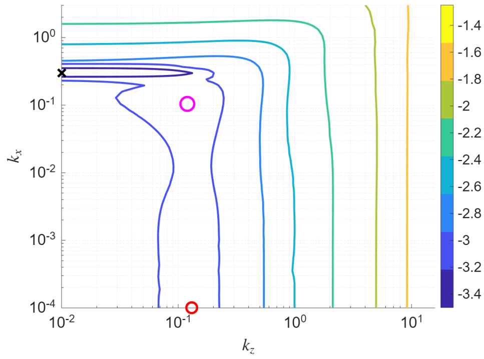

(b) $Re = 500$

Figure 3: Contour plots (in logarithmic scale) of $\sqrt{3}\|R\mathscr{H}_\nabla L\|^{-1}_{\mu_{\Delta_D}}(k_x, k_z)$ for Blasius flow. The X symbol denotes the most dominant mode, whereas the other modes from Table 1 are marked by colored circles (magenta - OW mode, black - TS mode, red - SPS mode).

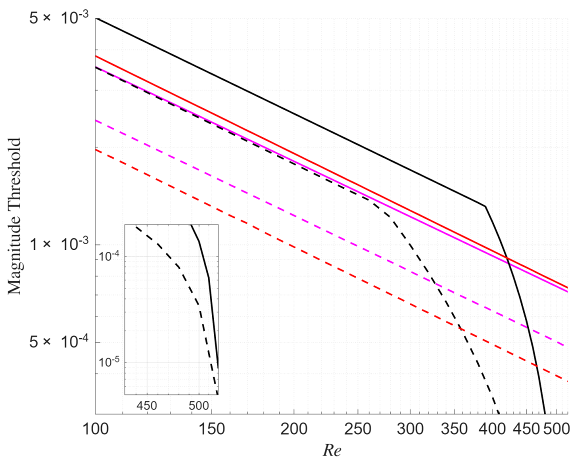

Figure 4: Evolution curves of imposed perturbation magnitude threshold due to flow structures associated with pre-selected modes of interest denoted in Table 1 (magenta - OW mode, black - TS mode, red - SPS mode) for Blasius base flow as a function of the Reynolds number in terms of our new threshold $\sqrt{3}\|R\mathscr{H}_\nabla L\|^{-1}_{\mu_{\Delta_D}}(k_x, k_z)$ (solid curves) and threshold determined by previous approach using repeated block uncertainty $\|\mathscr{H}_\nabla\|^{-1}_{\mu_{\Delta_r}}$ (dashed curves).

small perturbations, and thus results which match the predictions of LST are to be expected, where LST predicts that the least stable TS mode becomes unstable at $Re = 520$ (Schmid & Henningson, 2001). This result is consistent with our analysis in Frank-Shapir & Gluzman (2026) that uses other uncertainty structures.

At low, sub-critical Reynolds numbers, the lowest threshold is governed by the SPS and OW modes (for Reynolds numbers below 400 via our approach, and below 300 via the repeated block approach), which means that these modes require significantly smaller perturbations to lose stability than the TS mode. This result is consistent with previous literature, showing that bypass transition can be initiated by oblique (Schmid & Henningson, 1992; Berlin *et al.*, 1999; Elofsson & Alfredsson, 2000) and streaky structures (Andersson *et al.*, 1999, 2001; Brandt & Henningson, 2002). This also aligns with a few minimal seed studies that use nonlinear optimization to find the optimal perturbation that requires the least energy to induce turbulence at a specific Reynolds number. These studies often find that the optimal perturbation is characterized by a localized pair of vortices, tilted relative to the flow direction in an oblique fashion (Cherubini *et al.*, 2011; Beneitez *et al.*, 2019). The linear relationships that are observed in the log-log plot in Fig. 4 can be used to establish a power law relationship of the form $E_c \sim Re^{\gamma}$, where E_c is the critical perturbation kinetic energy required to trigger instability via our analysis for a particular mode. The obtained γ value from our analysis is slightly different for each mode, where $\gamma_{OW} = -1.94$ for OW mode, $\gamma_{TS} = -1.97$ for TS mode, and $\gamma_{SPS} = -2$ for the SPS mode. The linear relationships in the log-log plot hold up to $Re < 400$ via our approach (and for $Re < 300$ via repeated block approach), after which there is a rapid drop, which corresponds to a reduction of the critical perturbation energy required to lose stability.

CONCLUSIONS

We propose a new fixed-structure uncertainty that is interconnected with the linear frequency-response operator derived from the LNS equations, within a structured input-output framework, to quantify worst-case amplification via a computationally tractable SSV analysis. Our new representation of the interconnected system is designed to account for the structure of the advection term within a structured input-output framework via efficient computation. Using the structured small-gain theorem with our new fixed-structure uncertainty for analyzing flow stability as proposed in Frank-Shapir & Gluzman (2026), we provide an explicit threshold on the magnitude of velocity perturbations that assures flow stability.

Our new stability threshold is implemented on the Blasius boundary layer. We show that our approach yields less conservative bounds on disturbance magnitude than those approximated via the repeated block uncertainty modeling approach (Mushtaq *et al.*, 2024). The imposed disturbance thresholds decrease as the Reynolds number increases. For subcritical Reynolds numbers, the lowest threshold is imposed by oblique waves and spanwise periodic streaks. As the Reynolds number approaches the critical value predicted by linear stability theory, the lowest threshold is associated with the TS mode, imposing a threshold that tends to zero, recovering the expected LST result for infinitesimal disturbances.

REFERENCES

Andersson, P., Berggren, M. & Henningson, D. S. 1999 Optimal disturbances and bypass transition in boundary layers. *Phys. Fluids* **11** (1), 134–150.

Andersson, P., Brandt, L., Bottaro, A. & Henningson, D. S. 2001 On the breakdown of boundary layer streaks. *J. Fluid Mech.* **428**, 29–60.

Bamieh, B. & Dahleh, M. 2001 Energy amplification in channel flows with stochastic excitation. *Phys. Fluids* **13** (11), 3258–3269.

Beneitez, M., Duguet, Y., Schlatter, P. & Henningson, D. S. 2019 Edge tracking in spatially developing boundary layer flows. *J. Fluid Mech.* **881**, 164–181.

Berlin, S., Wiegel, M. & Henningson, D. S. 1999 Numerical and experimental investigations of oblique boundary layer transition. *J. Fluid Mech.* **393**, 23–57.

Bernstein, D. S. 2009 *Matrix Mathematics: Theory, Facts, and Formulas*. Princeton University Press.

Brandt, L. & Henningson, D. S. 2002 Transition of streamwise streaks in zero-pressure-gradient boundary layers. *J. Fluid Mech.* **472**, 229–261.

Cherubini, S., De Palma, P., Robinet, J.-C. & Bottaro, A. 2011 The minimal seed of turbulent transition in the boundary layer. *J. Fluid Mech.* **689**, 221–253.

Elofsson, P. A. & Alfredsson, P. H. 2000 An experimental study of oblique transition in a Blasius boundary layer flow. *Eur. J. Mech. B/Fluids* **19** (5), 615–636.

Farrell, B. F. & Ioannou, P. J. 1993 Stochastic forcing of the linearized Navier–Stokes equations. *Phys. Fluids A* **5** (11), 2600–2609.

Frank-Shapir, O. & Gluzman, I. 2025 Choosing between active and passive flow control via input-output analysis: Application to Couette flow. *IEEE Control Syst. Lett.* **9**, 715–720.

Frank-Shapir, O. & Gluzman, I. 2026 Stability analysis of transitional flows based on disturbance magnitude. *J. Fluid Mech.* **1030**, A8.

Gluzman, I. & Gayme, D. F. 2021 Input-output framework for actuated boundary layers. *Phys. Rev. Fluids* **6** (5), 053901.

Hwang, Y. & Cossu, C. 2010 Amplification of coherent streaks in the turbulent Couette flow: an input-output analysis at low Reynolds number. *J. Fluid Mech.* **643**, 333–348.

Jovanović, M. R. & Bamieh, B. 2004 Unstable modes versus non-normal modes in supercritical channel flows. In *Proc. Amer. Control Conf.*, pp. 2245–2250. Boston, MA: IEEE.

Jovanović, M. R. & Bamieh, B. 2005 Componentwise energy amplification in channel flows. *J. Fluid Mech.* **534**, 145–183.

Liu, C. & Gayme, D. F. 2020 An input–output based analysis of convective velocity in turbulent channels. *J. Fluid Mech.* **888**, A32.

Liu, C. & Gayme, D. F. 2021 Structured input–output analysis of transitional wall-bounded flows. *J. Fluid Mech.* **927**, A25.

Liu, C., Gluzman, I., Lozier, M., Midya, S., Gordeyev, S., Thomas, F. O. & Gayme, D. F. 2022 Spatial Input–Output Analysis of Actuated Turbulent Boundary Layers. *AIAA J.* **60** (11), 6313–6327.

Madhusudanan, A., Illingworth, S. J. & Marusic, I. 2019 Coherent large-scale structures from the linearized Navier–Stokes equations. *J. Fluid Mech.* **873**, 89–109.

McKeon, B. J. 2017 The engine behind (wall) turbulence: perspectives on scale interactions. *J. Fluid Mech.* **817**, P1.

McKeon, B. J. & Sharma, A. S. 2010 A critical-layer framework for turbulent pipe flow. *J. Fluid Mech.* **658**, 336–382.

McKeon, B. J., Sharma, A. S. & Jacobi, I. 2013 Experimental manipulation of wall turbulence: a systems approach. *Phys. Fluids* **25** (3), 031301.

Mushtaq, T., Bhattacharjee, D., Seiler, P. & Hemati, M. S. 2024 Structured singular value of a repeated complex full-block uncertainty. *Int. J. Robust Nonlinear Control* **34** (7), 4881–4897.

Mushtaq, T., Bhattacharjee, D., Seiler, P. J. & Hemati, M. 2023 Structured input-output tools for modal analysis of a transitional channel flow. In *AIAA SCITECH 2023 Forum*, p. 1805.

Packard, A. & Doyle, J. 1993 The complex structured singular value. *Automatica* **29** (1), 71–109.

Schlichting, H. & Gersten, K. 2016 *Boundary-Layer Theory*. Springer.

Schmid, P. J. & Henningson, D. S. 1992 A new mechanism for rapid transition involving a pair of oblique waves. *Phys. Fluids A* **4** (9), 1986–1989.

Schmid, P. J. & Henningson, D. S. 2001 *Stability and Transition in Shear Flows*, *Applied Mathematical Sciences*, vol. 142. New York: Springer.

Shuai, Y., Liu, C. & Gayme, D. F. 2023 Structured input–output analysis of oblique laminar–turbulent patterns in plane Couette–Poiseuille flow. *Int. J. Heat Fluid Flow* **103**, 109207.

Symon, S., Illingworth, S. J. & Marusic, I. 2021 Energy transfer in turbulent channel flows and implications for resolvent modelling. *J. Fluid Mech.* **911**, A3.

Zhou, K., Doyle, J. C. & Glover, K. 1995 *Robust and Optimal Control*. Upper Saddle River, NJ: Pearson.

A Derivation of Eq. (9)

Herein, we show the derivation of Eq. (9). First, we define the following matrices:

$$P = \begin{bmatrix} e_1 & e_4 & e_7 & e_2 & e_5 & e_8 & e_3 & e_6 & e_9 \end{bmatrix}^T. \quad (11)$$

Here, e_i is the i-th standard basis vector, defined by the i-th entry being equal to 1 and the rest of the entries being equal to 0. We define the block matrix $K \in \mathbb{R}^{rc\times rc}$ that consists of $r \times c$ blocks of matrices $E_{\ell m} \in \mathbb{R}^{c\times r}$, i.e.,

$$K_{r,c} = \begin{bmatrix} E_{11} & E_{12} & \cdots & E_{1c} \\ E_{21} & E_{22} & \cdots & E_{2c} \\ \vdots & \vdots & \ddots & \vdots \\ E_{r1} & E_{r2} & \cdots & E_{rc} \end{bmatrix}. \quad (12)$$

Each block $E_{\ell m} \in \mathbb{R}^{c\times r}$ is a matrix with elements $e_{i,j}$ satisfying:

$$e_{i,j} = \begin{cases} 1, & i = m,\, j = \ell \\ 0, & \text{else} \end{cases}. \quad (13)$$

The matrices L and R are defined below:

$$R = (I_{N_y} \otimes P)K_{N_y,9}, \;\; L = K_{3,N_y}(I_{N_y} \otimes \begin{bmatrix} I_3 & I_3 & I_3 \end{bmatrix}). \quad (14)$$

These matrices were designed to maintain the following relationship:

$$\Delta_{\mathbf{u}} \equiv \{\mathbf{U}_\Xi : \mathbf{U}_\Xi = L\mathbf{V}_\Xi R,\; \mathbf{V}_\Xi \in \Delta_D\}, \quad (15)$$

meaning that for every $\mathbf{U}_\Xi \in \Delta_{\mathbf{u}}$ there exists $\mathbf{V}_\Xi \in \Delta_D$ such that $\mathbf{U}_\Xi = L\mathbf{V}_\Xi R$. Furthermore, these matrices do not affect the nonzero entries of $\mathbf{V}_\Xi$, only reordering them to obtain the diagonal structure Δ_D. The dimensions of these matrices are defined by the number of discretization points we used, denoted as N_y. Herein, we use $\mathbf{U}_\Xi \in \mathbb{C}^{3N_y\times 9N_y}$, $L \in \mathbb{R}^{3N_y\times 9N_y}$, $R \in \mathbb{R}^{9N_y\times 9N_y}$, and $\mathbf{V}_\Xi \in \mathbb{C}^{9N_y\times 9N_y}$.

The determinant condition in the SSV definition shown in Eq. (4) becomes:

$$\det[I - \mathscr{H}_\nabla \mathbf{U}_\Xi] = \det[I - \mathscr{H}_\nabla L\mathbf{V}_\Xi R]. \quad (16)$$

By employing the Weinstein–Aronszajn determinant identity (see Bernstein (2009, Corollary 2.8.5.)), we obtain:

$$\det[I - \mathscr{H}_\nabla L\mathbf{V}_\Xi R] = \det[I - R\mathscr{H}_\nabla L\mathbf{V}_\Xi]. \quad (17)$$

Next, we relate the singular values of two uncertainty matrices $\mathbf{U}_\Xi \in \Delta_{\mathbf{u}}$ and $\mathbf{V}_\Xi \in \Delta_D$. It was shown in Frank-Shapir & Gluzman (2026) that

$$\bar{\sigma}(\mathbf{U}_\Xi) = \max_i \sqrt{|u_{\xi_i}|^2 + |v_{\xi_i}|^2 + |w_{\xi_i}|^2}. \quad (18)$$

As in Eq. (7), $u_\xi, v_\xi, w_\xi \in \mathbb{C}^{N_y\times 1}$ represent discretized versions of the perturbation velocity components. The notation u_{ξ_i} (and similarly for the two other velocity components) denotes the i-th entry of u_ξ in the discretized domain, which contains N_y entries. Since $\mathbf{V}_\Xi$ is a diagonal matrix of reorganized entries from $\mathbf{U}_\Xi$, its largest singular value is

$$\bar{\sigma}(\mathbf{V}_\Xi) = \max_i \{|u_{\xi_i}|, |v_{\xi_i}|, |w_{\xi_i}|\}. \quad (19)$$

It is clear that

$$\bar{\sigma}(\mathbf{U}_\Xi) \le \sqrt{3}\bar{\sigma}(\mathbf{V}_\Xi). \quad (20)$$

Using the determinant equality in Eq. (17), the singular value relation in Eq. (20), within the minimization problem in Eq. (4), we obtain

$$\frac{1}{\sqrt{3}}\mu_{\Delta_D}(R\mathscr{H}_\nabla L) \le \mu_{\Delta_{\mathbf{u}}}(\mathscr{H}_\nabla). \quad (21)$$

Then, based on Eq. (5), we obtain

$$\frac{1}{\sqrt{3}}\|R\mathscr{H}_\nabla L\|_{\mu_{\Delta_D}} \le \|\mathscr{H}_\nabla\|_{\mu_{\Delta_{\mathbf{u}}}}. \quad (22)$$

Lastly, we obtain Eq. (9) by computing the inverse of Eq. (22).